Problems with the interpretation of the ^{10}He ground state

L. V. Grigorenko[1,2,3] and M. V. Zhukov[4]

[1]*Flerov Laboratory of Nuclear Reactions, JINR, RU-141980 Dubna, Russia*

[2]*Gesellschaft für Schwerionenforschung mbH, Planckstrasse 1, D-64291, Darmstadt, Germany*

[3]*RRC "The Kurchatov Institute", Kurchatov sq. 1, RU-123182 Moscow, Russia*

[4]*Fundamental Physics, Chalmers University of Technology, S-41296 Göteborg, Sweden*

(Received 28 September 2007; revised manuscript received 1 January 2008; published 27 March 2008)

The continuum of the ^{10}He nucleus is studied theoretically in a three-body ^{8}He+n+n model based on recent information concerning the ^{9}He spectrum [M. S. Golovkov *et al.*, Phys. Rev. C **76**, 021605(R) (2007)]. The ^{10}He ground state (g.s.) candidate with structure $[p_{1/2}]^2$ for new g.s. energy of ^{9}He is predicted to be at about 2.0–2.3 MeV. The peak in the cross section associated with this state may be shifted to a lower energy (e.g., $\sim$1.2 MeV) when ^{10}He is populated in reactions with ^{11}Li due to a peculiar reaction mechanism. Formation of the low-energy ($E < 250$ keV) "alternative" ground state with structure $[s_{1/2}]^2$ is highly probable in ^{10}He when there is considerable attraction (e.g., $a < -5$ fm) in the s-wave ^{9}He channel, whose properties are still quite uncertain. This result either questions the existing experimental low-energy spectrum of ^{10}He or places a limit on the scattering length in the ^{9}He channel, which contradicts existing data.

DOI: 10.1103/PhysRevC.77.034611 PACS number(s): 21.60.Gx, 21.45.−v, 21.10.Dr, 27.20.+n

I. INTRODUCTION

The first, at that time theoretical, attempt to study ^{10}He was undertaken at the end of the 1960s [1]. In that work, the possibility of the nuclear-stable ^{10}He existence was investigated in the microscopic ten-body hyperspherical harmonic (HH) model. However, until now the ^{10}He nucleus remains a relatively poorly studied system. After it became clear that ^{10}He is nuclear unstable [2] and the ground state properties of ^{9}He were defined [3,4], it became possible to predict theoretically the ground state of ^{10}He as a narrow three-body ^{8}He+n+n resonance. The ground state resonance was found with $E \sim 0.7$–0.9, $\Gamma \sim 0.1$–0.3 MeV [5], for valence neutrons populating mainly the $[p_{1/2}]^2$ configuration (the energy E in the present work is always given relative to the three-body ^{8}He+n+n threshold). These predictions were soon confirmed experimentally: $E = 1.2(3), \Gamma < 1.2$ MeV [6], $E = 1.07(7), \Gamma = 0.3(2)$ MeV [7,8], and $E = 1.7 \pm 0.3 \pm 0.3$ MeV [9].

A new possible theoretical understanding of ^{10}He was proposed after the existence of a virtual state in ^{9}He was demonstrated by Chen *et al.* in Ref. [10]. An *upper* limit for scattering length $a < -10$ fm was established in that experimental work. For such an attractive s-wave interaction in ^{9}He, Aoyama predicted [11] the existence of a narrow near-threshold 0^+ state in ^{10}He ($E = 0.05, \Gamma = 0.21$ MeV) with the $[s_{1/2}]^2$ structure in addition to the $[p_{1/2}]^2$ state (calculated in that work to be at about 1.7 MeV). Concerning evident discrepancy with the experimental data, Aoyama suggested [11] that the ground state (g.s.) of ^{10}He had not been observed so far, and the state at $\sim$1.3 MeV is actually the first excited state. However, no possible explanation was proposed in Ref. [11] for why the $[s_{1/2}]^2$ g.s. was missed in experiments.

In a recent experiment by Golovkov *et al.* [12] at the Dubna radioactive beam facility ACCULINNA, the low-lying spectrum of ^{9}He was revised, providing a higher position of the $p_{1/2}$ state than given in previous studies. A broad $p_{1/2}$ state was observed at about 2 MeV instead of the (presumably) $p_{1/2}$-$p_{3/2}$ doublet of narrow states at 1.27 and 2.4 MeV as seen in Refs. [3,4,8]. The experiment [12] also claims a unique spin-parity identification below 5 MeV. The presence of the $s_{1/2}$ contribution is evident in the data [12], but the exact nature of this contribution is still unclear, i.e., whether it is a virtual state with a considerably large negative scattering length or just a smooth nonresonant background. A relaxed *lower* limit for scattering length $a > -20$ fm was established in that work. These new data should have a strong impact on the calculated properties of ^{10}He, which inspired us to "revisit" the issue.

In the present work, we study the question in theoretical models, which are schematic but have a clear relevance to real possible reaction mechanisms of the ^{10}He continuum population. The approach of Ref. [11] provided only energies and widths of the states. In contrast, we are interested in the observable consequences of the "coexistence" of the $J^\pi = 0^+$ states with structures $[s_{1/2}]^2$ and $[p_{1/2}]^2$ in the ^{10}He spectrum. We demonstrate that this problem has a key importance for understanding the observable properties of ^{10}He. We conclude that the simultaneous consistent understanding of the low-lying spectra of ^{9}He and ^{10}He is still a challenge, both theoretically and experimentally.

The unit system $\hbar = c = 1$ is used in this work.

II. THEORETICAL MODEL

To choose the interactions in this work, we generally follow the prescription of the three-cluster ^{8}He+n+n calculations of Ref. [5] with appropriate modifications of potentials. From the set of core-n potentials tested in Ref. [5], we selected one (denoted there as "I2"). Other choices do not change qualitatively the result and quantitatively are quite close. The potential is parametrized by the Gaussian form factor

$$V^l_{c,ls}(r) = V^l_{c,ls} \exp\left[-r^2/r_0^2\right],$$

with $r_0 = 3.4$ fm. The depths of the d-wave potential $V_c^2 = -33$ MeV and the (ls) component in the p-wave, $V_{ls}^1 = 10$ MeV, are the same as in the original paper. The inverse (ls) forces were used in Ref. [5] in the p-wave to account for the occupied $p_{3/2}$ subshell in the ^{8}He core. The interaction in the s-wave ^{8}He-n channel was purely repulsive in Ref. [5] to account for an occupied $s_{1/2}$ shell in the ^{8}He core. Central potential parameters in s- and p-waves V_c^0 and V_c^1 are being varied to clarify different aspects of the system dynamics. To manage the occupied $s_{1/2}$ state in ^{8}He in this work, an additional repulsive core is introduced in the s-wave with parameters $r_0(\text{core}) = 2.35$ fm and $V_c^0(\text{core}) = 75$ MeV.

With the above potential, the d-wave state in ^{9}He is found at 4.8 MeV, which is consistent with the the experimental data [3,8,12] giving values in the range 4.2–4.9 MeV for the $d_{5/2}$ state. With $V_c^1 = -10$ MeV (the value from the Ref. [5]), the $p_{1/2}$ state is obtained at 0.74 MeV. This value is different from the value 1.15 MeV quoted in Ref. [5], where this is the energy at which the phase shift passes $\pi/2$. In this work, we have to deal also with broad states, where the phase shift does not reach $\pi/2$. Thus, we define the resonance position for the two-body subsystem by the "observable value" (peak in the elastic cross section) and define the width as the full width at half maximum (FWHM) for this peak.

The realistic soft-core potential [13] is used in the n-n subsystem also following Ref. [5].

To study qualitatively a possible influence of the reaction mechanism, we follow the approach of paper [14] to the exotic ^{5}H system. We introduce a compact source function $\Phi(\rho, \Omega_\rho)$ in the right-hand side of the three-body Schrödinger equation and solve the inhomogeneous system of equations

$$(\hat{H} - E)\Psi_E^{(+)}(\rho, \Omega_\rho) = \Phi(\rho, \Omega_\rho), \tag{1}$$

$$\begin{aligned} \hat{H} &= \hat{T} + \hat{V}_{cn}(\mathbf{r}_{cn_1}) + \hat{V}_{cn}(\mathbf{r}_{cn_2}) + \hat{V}_{nn}(\mathbf{r}_{n_1n_2}), \\ \rho^2 &= \frac{8}{10}\left(r_{cn_1}^2 + r_{cn_2}^2\right) + \frac{1}{10}r_{n_1n_2}^2 = \frac{1}{2}X^2 + \frac{8}{5}Y^2, \end{aligned} \tag{2}$$

for pure outgoing wave boundary conditions, utilizing the hyperspherical harmonic (HH) method. The coordinates used are shown in Fig. 1. The hyperradial components $\chi_{K\gamma}^{(+)}(\rho)$ of the wave function (WF)

$$\Psi_E^{(+)}(\rho, \Omega_\rho) = \rho^{-5/2} \sum_{K\gamma}^{K_{\max}} \chi_{K\gamma}^{(+)}(\varkappa\rho)\, \mathcal{J}_{K\gamma}^{JM}(\Omega_\rho)$$

are matched to Riccati-Bessel functions of half-integer index $\mathcal{H}_{K+3/2}^{(+)}$. Functions $\mathcal{H}^{(+)}$ have the asymptotic behavior $\exp[i\varkappa\rho]$, where $\varkappa = \sqrt{2ME}$ (M is a nucleon mass), describing the partial outgoing waves for hyperspherical equations. The value $K_{\max}$ truncates the hyperspherical expansion. The hypermoment $\varkappa$ is expressed via the energies of the subsystems E_x, E_y or via Jacobi momenta k_x, k_y conjugated to Jacobi coordinates X, Y:

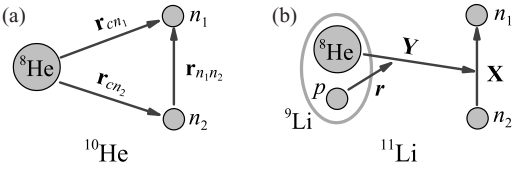

FIG. 1. Coordinate sets used in this paper. Panel (b) illustrates a proton removal from ^{11}Li as a method to populate ^{10}He.

$$\begin{aligned} &\mathbf{k}_x = \tfrac{1}{2}\left(\mathbf{k}_{n_1} - \mathbf{k}_{n_2}\right), \quad \mathbf{k}_y = \tfrac{4}{5}\left(\mathbf{k}_{n_1} + \mathbf{k}_{n_2}\right) - \tfrac{1}{5}\mathbf{k}_c, \\ &\varkappa^2 = 2ME = 2M(E_x + E_y) = 2k_x^2 + \tfrac{5}{8}k_y^2. \end{aligned} \tag{3}$$

The Jacobi variables are given in the "T" Jacobi system. A more detailed picture of Jacobi coordinates for coordinate and momentum spaces in "T" and "Y" Jacobi systems can be found in Fig. 13.

The set of coupled equations for functions $\chi^{(+)}$ has the form

$$\begin{aligned} &\left[\frac{d^2}{d\rho^2} - \frac{\mathcal{L}(\mathcal{L}+1)}{\rho^2} + 2M\{E - V_{K\gamma,K\gamma}(\rho)\}\right]\chi_{K\gamma}^{(+)}(\rho) \\ &\quad = 2M\sum_{K'\gamma'} V_{K\gamma,K'\gamma'}(\rho)\chi_{K'\gamma'}^{(+)}(\rho) + 2M\,\Phi_{K\gamma}(\rho), \end{aligned} \tag{4}$$

$$\begin{aligned} &V_{K\gamma,K'\gamma'}(\rho) \\ &\quad = \int d\Omega_\rho\, \mathcal{J}_{K'\gamma'}^{JM*}(\Omega_\rho) \sum_{i<j} V_{ij}(\mathbf{r}_{ij})\, \mathcal{J}_{K\gamma}^{JM}(\Omega_\rho), \\ &\Phi_{K\gamma}(\rho) \\ &\quad = \rho^{5/2}\int d\Omega_\rho\, \mathcal{J}_{K\gamma}^{JM*}(\Omega_\rho)\Phi(\rho, \Omega_\rho), \end{aligned} \tag{5}$$

where $\mathcal{L} = K + 3/2$ and $V_{K\gamma,K'\gamma'}(\rho)$ are matrix elements of the sum of the pairwise potentials referred to in this work as three-body potentials.

A more detailed account of the method can be found, e.g., in Ref. [14]. It is shown there that the method is consistent with "sudden removal" approximation for high-energy fragmentation reactions. The development of the technically similar approach in the framework of the distorted-wave Born approximation (DWBA) theory, applied to the inelastic processes in the transfer reactions, can be found in Ref. [15].

We used two different sources, consistent with different reaction conditions. One is a "narrow" source with a Gaussian form factor,

$$\Phi(\rho, \Omega_\rho) = \exp\left[-\rho^2/\rho_0^2\right] \sum_{K=0,2\ S=0} \mathcal{J}_{K\gamma}^{JM}(\Omega_\rho), \tag{6}$$

where $\rho_0 = 4.1$ fm provides the source rms radius $\langle\rho\rangle = 5$ fm. This is a typical radius for the "reaction volume" for ordinary nuclei. The source populates only the lowest hyperspherical components of the WF ($K = 0, 2$). This qualitatively corresponds to the population of the $[s]^2$ and $[p]^2$ shell model configurations in the ^{10}He nucleus, which are expected to be the most important for the low-energy part of the spectrum. The condition $S = 0$ is qualitatively consistent with the mechanism of transfer reactions, where the ^{10}He states are populated by transferring a two-neutron pair (with total spin equal zero) to the ^{8}He core. In such reactions, the $\Delta S = 1$ transfer is strongly suppressed and the $\Delta S = 0$ transfer is a very reliable assumption.

The other choice of the source is more reaction specific. When ^{10}He is produced from ^{11}Li in a process that can be approximated as a sudden proton removal from the ^{9}Li core,

the source term $\Phi(\rho, \Omega_\rho)$ should contain the Fourier transform of the overlap integral between the ^{8}He WF $\Psi_{^8\mathrm{He}}$, the spin-isospin function of the removed proton χ_p, and the ^{11}Li wave function over the radius vector $\mathbf{r}$ between the removed proton and the center of mass of ^{10}He [see Fig. 1(b)]:

$$\Phi(\rho, \Omega_\rho) = \int d\mathbf{r}\, e^{i\mathbf{q}\mathbf{r}} \langle \Psi_{^8\mathrm{He}} \chi_p | \Psi_{^{11}\mathrm{Li}} \rangle . \qquad (7)$$

In general, this quantity is a complicated function of the recoil momentum vector $\mathbf{q}$, transferred to the ^{10}He system in the proton removal process. However, if the recoil momentum is relatively small (e.g. $q < 100$–150 MeV/c), and the internal energy of ^{10}He is small, one can neglect this dependence (see Ref. [14] for details). It can be shown that in this case partial hyperspherical components of the source function are well approximated by the corresponding components of the ^{11}Li WF. Thus, this type of calculation is further referred to as the "^{11}Li source." The ^{11}Li WF was taken from an analytical parametrization developed in Ref. [16] taking into account the broad range of experimental information on this nucleus. The dominant $[s_{1/2}]^2$ and $[p_{1/2}]^2$ configurations are populated by the ^{11}Li source with almost equal probabilities. The rms radius of such a source function $\langle \rho \rangle = 9.5$ fm is enormous compared to typical nuclear sizes.

In the approach with the source function of Eq. (1), the cross section for population of the ^{10}He continuum is proportional to the outgoing flux of the three particles on a hypersphere of some large radius $\rho = \rho_{\max}$:

$$\frac{d\sigma}{dE} \sim \frac{1}{M} \mathrm{Im} \int d\Omega_\rho \, \Psi_E^{(+)\dagger} \rho^{5/2} \frac{d}{d\rho} \rho^{5/2} \Psi_E^{(+)} \Big|_{\rho=\rho_{\max}} . \qquad (8)$$

Differentials of this flux on the hypersphere provide angular and energy distributions among the decay products at given decay energy E (see Ref. [14] for details of correlation calculations).

III. CALCULATIONS

A. Basis size convergence

The HH calculations in our method can be performed with $K_{\max} = 24$–26. Such basis sizes could be insufficient for obtaining a good energy convergence of calculations in some complicated cases. The basis size can be further increased effectively using the adiabatic procedure based on the so-called Feshbach reduction (FR) [17]. Feshbach reduction eliminates from the total WF, $\Psi = \Psi_p + \Psi_q$, an arbitrary subspace q using the Green's function of this subspace:

$$H_p = T_p + V_p - V_{pq} G_q V_{pq}.$$

In certain adiabatic approximations, we can assume that the radial part of the kinetic energy is small under the centrifugal barrier in the channels with high centrifugal barriers and can be approximated by a constant. In this approximation, the FR procedure is reduced to the construction of effective three-body interactions $V^{\mathrm{eff}}_{K\gamma,K'\gamma'}$ by matrix operations, that is,

$$G^{-1}_{K\gamma,K'\gamma'} = (H - E)_{K\gamma,K'\gamma'} = V_{K\gamma,K'\gamma'} + \left[E_f - E + \frac{(K+3/2)(K+5/2)}{2M\rho^2} \right] \delta_{K\gamma,K'\gamma'},$$

$$V^{\mathrm{eff}}_{K\gamma,K'\gamma'} = V_{K\gamma,K'\gamma'} - \sum V_{K\gamma,\bar{K}\bar{\gamma}} G_{\bar{K}\bar{\gamma},\bar{K}'\bar{\gamma}'} V_{\bar{K}'\bar{\gamma}',K'\gamma'}.$$

Summation over indexes with overbar is made for eliminated channels. We take the Feshbach energy E_f in our calculations as $E_f \equiv E$.

The reliability of the FR procedure can be checked in two ways. We can compare dynamic calculations for some large $K_{\max}$ with the "reduced" calculations $K_{\max} \to K_{\mathrm{FR}}$ (with much smaller dynamic basis size K_{FR}), and in principle they should coincide. Calculations show that for ^{10}He starting from $K_{\max} = 26$, we get practically the same result down to $K_{\mathrm{FR}} = 10$. The other way to check the procedure's reliability is the following. We can start FR with some quite large fixed $K_{\max}$ (e.g., from $K_{\max} = 100$ in this work), make the reduction to a different $K_{\mathrm{FR}} \leqslant 26$, and perform dynamic calculations with each of them. Again the results are found to coincide precisely for $K_{\mathrm{FR}} \geqslant 10$. Thus the FR procedure is found to be reliable for performing most of the calculations (except those for correlations) with the dynamic basis size $K_{\mathrm{FR}} = 12$, varying the effective basis size $K_{\max}$ when necessary.

The cross section convergence with the increase of the effective hyperspherical basis size is demonstrated in Fig. 2. For a resonance peak with the $[p_{1/2}]^2$ structure, the convergence

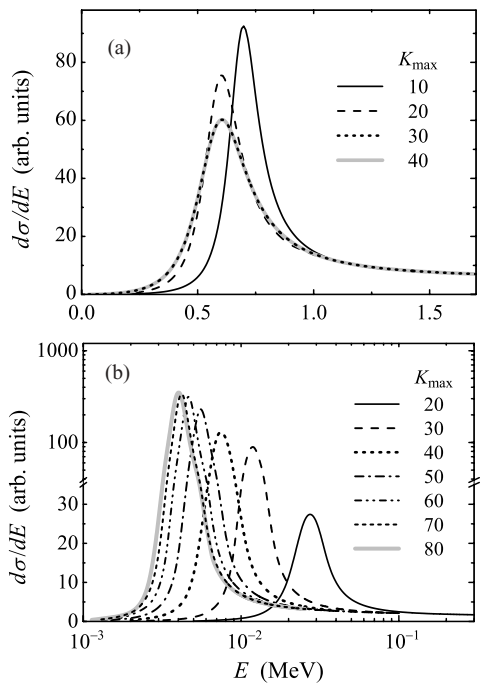

FIG. 2. Convergence of calculations as a function of $K_{\max}$ (the value truncating the hyperspherical basis). Calculations with narrow source. (a) Resonance peak with $[p_{1/2}]^2$ structure. The ^{8}He-n potential parameters are $V_c^0 = 0$, $V_c^1 = -10$ MeV. (b) Resonance peak with $[s_{1/2}]^2$ structure. Parameters are $V_c^0 = -26.93$ MeV (this corresponds to $a = -15$ fm in ^{9}He), $V_c^1 = -4.5$ MeV.

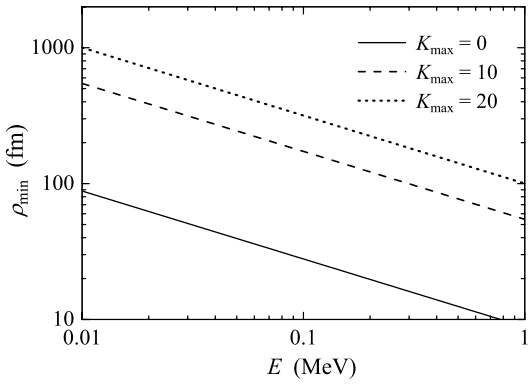

FIG. 3. Hyperradius of the classical turning point ρ_{min} for hyperradial centrifugal barriers in channels with different K values.

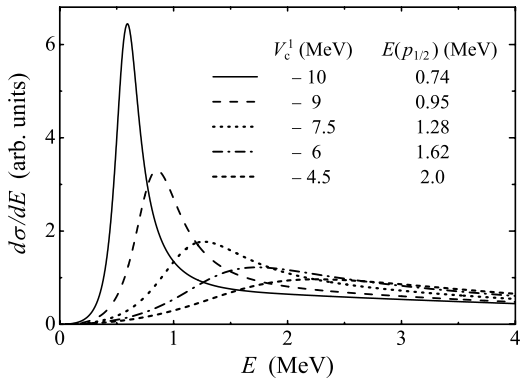

FIG. 4. Behavior of the ^{10}He spectrum with decrease of the p-wave potential depth V_c^1. The corresponding $p_{1/2}$ state energies $E(p_{1/2})$ in ^{9}He relative to the ^{8}He-n threshold are shown in the legend. Calculations with narrow source.

is reliably achieved by $K_{max} = 30$. However, for a state with the $[s_{1/2}]^2$ structure, more efforts are required to achieve the convergence (because very close to the threshold, even a minor variation of the energy becomes noticeable). We intentionally demonstrate in Fig. 2(b) the calculation, which is numerically more complicated than the others considered in the paper. Namely, when the s-wave potential in the ^{8}He-n subsystem is taken to provide the scattering length $a = -15$ fm, the resonance peak in ^{10}He is obtained at $E = 4$ keV with $\Gamma = 0.7$ keV. The basis size $K_{max} = 80$ is required in such a case to obtain the convergence.

Another aspect of the basis size choice is connected with the radial extent of the calculations ρ_{max}. The formulation of the cross section calculations in the form (8) implies that the WF resides at ρ_{max} in the classically allowed region. Taking into account the character of the hyperspherical centrifugal barrier (4), this requires a very large radial extent for large basis sizes. Figure 3 provides the estimates of the minimally required values of ρ_{max} to satisfy this condition for different K values. So, we used $\rho_{max} \sim 300$–500 fm for calculations of the $[p_{1/2}]^2$ states and $\rho_{max} \sim 1000$–2000 fm for the extreme low-energy calculations of the $[s_{1/2}]^2$ states.

B. Sensitivity to the p wave in ^{9}He

The ground state resonance properties were predicted as $E \sim 0.7$–0.9 MeV, $\Gamma \sim 0.1$–0.3 MeV in Ref. [5]. Within the approach used in that work, we first of all reproduce the results of previous studies. The calculation with model parameters consistent with those of Ref. [5] is shown in Fig. 4, by the solid curve. The peak position is somewhat lower than in Ref. [5] ($E = 0.6$ MeV, $\Gamma = 0.27$ MeV) which is connected to the larger basis size [see Fig. 2(a)]. Note that $K_{max} = 8$ was used in Ref. [5].

The evolution of the cross section with the decrease of the p-wave interaction from the value adopted in Ref. [5] [$V_c^1 = -10$ MeV, which provided the energy of the $p_{1/2}$ state $E(p_{1/2}) = 0.74$ MeV] to a value providing the ^{9}He g.s. to be at about 2 MeV ($V_c^1 = -4.5$ MeV) is shown in Fig. 4 for the narrow source function. The new peak position for the ^{10}He population cross section is at $E = 2.3$ MeV. The impact of this change is drastic: the narrow ^{10}He g.s. peak is practically "dissolved" as the system becomes less bound: e.g., the width of the peak can no longer be well defined as FWHM

C. Sensitivity to the reaction mechanism

The evolution of cases with different p-wave interactions with increase of the s-wave interaction is shown in Fig. 5 for the narrow and broad source functions, which should simulate different reaction conditions. We first discuss the sensitivity of the cross section to the reaction mechanism.

The narrow ground state in ^{10}He is not significantly sensitive to the reaction mechanism. This can be seen by comparing Figs. 5(a) and 5(d): the difference of the curves of the same style in the upper and lower panels is quantitative, not qualitative. This is an expected result, as the narrow states have a sufficiently large lifetimes to "forget" how they were populated and thus lose the sensitivity to the population mechanism.

When the state is above 1 MeV, the width becomes comparable to 1 MeV, and the dependence on the source function is considerable [Figs. 5(b) and 5(e)]. In the case of even higher ^{10}He g.s., the calculations with narrow and broad sources have very little in common [Figs. 5(c) and 5(f)]. According to the recent result [12], the cases (c) and (f) should be regarded as the most realistic. Thus, peculiarities of the reaction mechanism could be a problem in interpreting the ^{10}He spectra.

D. Sensitivity to the s wave in ^{9}He

It can be seen from Fig. 5 that for relatively weak s-wave attraction, the g.s. peak is shifted to lower energies with minimal distortion. However, as the s-wave attraction becomes stronger, the threshold peculiarity is formed in the spectrum. With the further increase of the s-wave interaction, this peculiarity is transformed into a very sharp low-energy ($E < 300$ keV) peak. The WF at this peak has a practically pure $[s_{1/2}]^2$ structure, and we characterize it as a "three-body virtual state."

In using the term "three-body virtual state" we have two things in mind: this is an s-wave state built upon the virtual states in all the subsystems, and this state has distinct

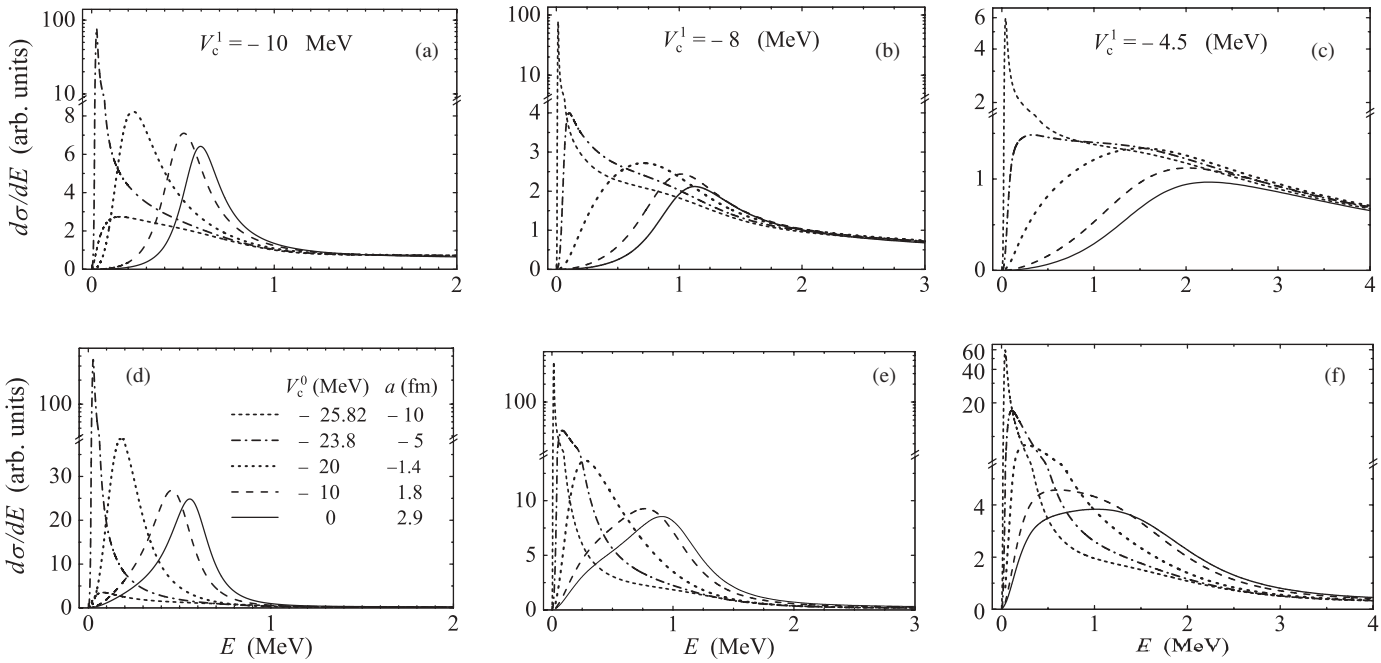

FIG. 5. Behavior of the ^{10}He spectrum with increase of the s-wave interaction [legend, the same for all panels, is shown in panel (d)]. The first row shows the narrow source case, the second row is for the broad (^{11}Li) source. In the first column, calculations for p-wave potential $V_c^1 = -10$ MeV ($p_{1/2}$ state at 0.74 MeV, as in calculations of Ref. [5]); in the second column for $V_c^1 = -8$ MeV ($p_{1/2}$ state at 1.16 MeV, close to 1.27 MeV, as in experiment [8]); in the third column for $V_c^1 = -4.5$ MeV ($p_{1/2}$ state at 2 MeV, as in experiment [12]). Smooth behavior of the short-dashed curves ($V_c^0 = -25.82$ MeV, $a = -10$ fm) in panels (a) and (d) is connected to the fact that the bound 0^+ state of ^{10}He is formed with binding energy ≈60 keV. Note the change of the scales on the vertical axes to logarithmic.

properties compared to those of ordinary resonant three-body states (relevant discussion of Efimov-like three-body virtual excitations can be found in Ref. [18]).

The ordinary two-body virtual states are typically characterized in two ways: (i) as a negative energy pole on the second Riemann sheet or (ii) as a threshold peculiarity[1] preceding the formation of the bound state in the case of absence of the potential barrier. The pole behavior in three-body systems has been studied in a number of works with the emphasis on the possible similarities with two-body virtual state pole behavior [11,19–22]. In paper [22], the possibility of such behavior in the three-body s-wave system was shown for interactions with certain extreme properties. Observable consequences of such a pole behavior in the three-body systems remain unclear. Our way of thinking about the three-body virtual state is more relevant to the second characteristic of the two-body virtual state, which is related to its observables.

For the relatively strong s-wave interaction in the ^{8}He-n subsystem (namely, such that the scattering length $a < -5$ fm), we unavoidably (means independently of the structure and reaction mechanism details) get a sharp peak in the cross section with an energy of less than 0.3 MeV and with a dominating $[s_{1/2}]^2$ configuration. The stable formation of the low-energy peak at certain strengths of the attractive s-wave interaction in ^{9}He is an important dynamical feature of the ^{10}He system, which makes us optimistic about the predictive abilities of theoretical models in this situation. The extreme low-energy peaks could hardly be consistent with the experimental data [6]; the discussion of the issue is provided below in Sec. IV A.

It can be noticed that in the case of the very narrow three-body virtual state formation, some structure can be seen as a "shoulder" on the right slope of the $[s_{1/2}]^2$ peak. It is possible to understand that this structure corresponds to the state with the $[p_{1/2}]^2$ structure which becomes sufficiently well split from the $[s_{1/2}]^2$ state and even preserves the position typical for the $V_c^0 = 0$ case. The analysis of the partial decomposition of the cross section provided in Fig. 6 indicates that this is generally true. However, the $[p_{1/2}]^2$ contribution to WF is considerably broadened and reduced in absolute value compared to the case when there was no s-wave attraction. To understand Fig. 6, it is useful to note that at the "shell model language" the $K = 0$ configuration is a pure $[s_{1/2}]^2$, while the $K = 2$ components (for p-shell nuclei) are mainly decomposed as

$$|K = 2, L = 0\rangle = \sqrt{1/3}\,[p_{1/2}]^2 + \sqrt{2/3}\,[p_{3/2}]^2,$$
$$|K = 2, L = 1\rangle = \sqrt{2/3}\,[p_{1/2}]^2 - \sqrt{1/3}\,[p_{3/2}]^2.$$

The weight of the $[p_{1/2}]^2$ configuration relative to the total weight of $[p_{1/2}]^2$ and $[p_{3/2}]^2$ configurations varies as 80–90% in different calculations of the p-wave state.

E. Properties of the three-body virtual state

An important feature that differentiates a three-body virtual state (the one with a dominant $[s_{1/2}]^2$ structure) from the

[1]For example, in the inelastic process the virtual state is seen as a near threshold peak with non-Lorencian shape.

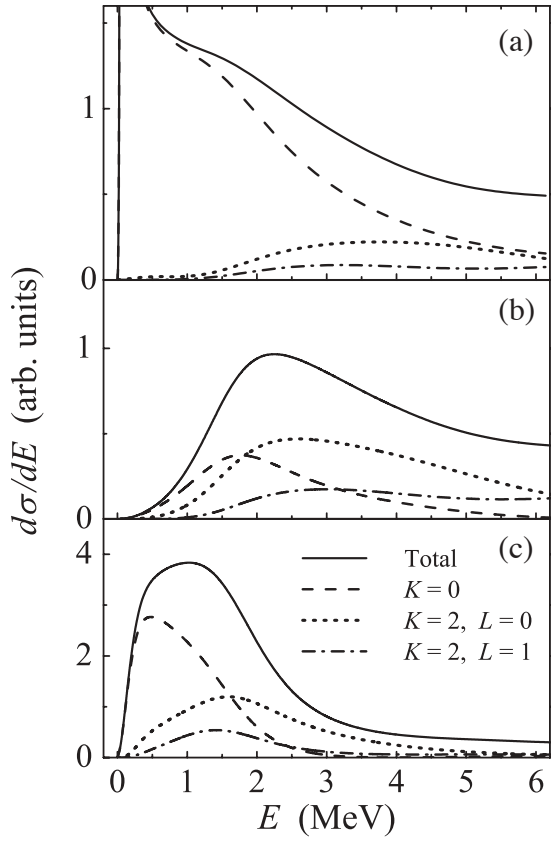

FIG. 6. Partial decomposition of the cross section; dashed, dotted and dash-dotted curves provide contributions of the main WF components. Calculations are with p-wave resonance in ^{9}He at 2 MeV ($V_c^1 = -4.5$ MeV). Different panels correspond to (a) $V_c^0 = -25.82$ ($a = -10$ fm), narrow source; (b) $V_c^0 = 0$ narrow source, and (c) $V_c^0 = 0$, ^{11}Li source.

ordinary two-body virtual state is evident from the structure of Eq. (4). This feature has been discussed in an exploratory fashion in the past (e.g., Ref. [20]), but it seems that in ^{10}He this kind of physics could become really accessible for observation. The state with the $[s_{1/2}]^2$ structure should be characterized by domination of the component with the lowest possible value of the generalized angular momentum $K = 0$. However, the centrifugal barrier $\mathcal{L}(\mathcal{L}+1)/2M\rho^2$ is not zero even in the channel with $K = 0$, as it depends on the "effective angular momentum" $\mathcal{L} = K + 3/2$. This means that the low-energy three-body virtual state may exist in the form of a real resonance peak, not a threshold peculiarity as the two-body virtual state. It is also easy to demonstrate that the low-energy behavior of the inelastic cross section for the population of the three-body continuum is

$$d\sigma/dE \propto E^2,$$

in contrast with the two-body inelastic cross section which has a square root peculiarity in the case of the virtual state

$$d\sigma/dE \propto \sqrt{E}.$$

Such a behavior should in principle distinctly separate the three-body virtual state peak from zero energy. Such a separation was demonstrated in Ref. [20] for a toy model of the $[s^2]$ state for the "Borromean system."[2] Namely, it was shown in the analytical continuation of coupling constant (ACCC) method that the pole trajectories in the case of the $[s^2]$ three-body state are analogous to the trajectories in the system with barriers, while for the two-body virtual states they are qualitatively different.

The mentioned features, however, do not mean that a three-body virtual state is an ordinary resonance state; there is an important difference. It is known that the resonance behavior is connected to time delays in the propagation of particles (and corresponding time-dependent theory can be formulated in these terms). Ordinarily, the time delay is connected to the confinement of particles inside the potential barrier, and their WF is localized inside the potential well, displaying the "quasibound" nature of such resonances. For a virtual state, the time delay is not connected with a barrier and the tight spacial localization of particles close to each other. It is connected with the *slow* motion of particles in the volume of a sphere with a *large* radius (comparable to the scattering length). In the three-body case, the hyperspherical centrifugal barrier $\mathcal{L}(\mathcal{L}+1)/2M\rho^2$ has an effective collective nature; it is clear that individual nucleons in the $[s_{1/2}]^2$ configuration do not "see" any barriers. The time delay is connected therefore to the simultaneous presence of two valence nucleons in the volume around the core, associated with scattering lengths, which means a peripheral nature of such a state.

The peripheral character of the state presumes a different character of the dependence of the resonance width on energy than the behavior which could be expected for "typical" barrier penetration. We can take, for example, the calculated properties of the ^{10}He g.s. in the case $a = -15$ fm ($E = 4$ keV, $\Gamma = 0.7$ keV, see Fig. 2) and deduce the "channel radius" $\rho_{\rm ch}$ using for the penetration an expression analogous to the single-channel R-matrix formula. It can be found in Ref. [24]:

$$\Gamma = \frac{1}{M\rho_{\rm ch}^2}\,\frac{2}{\pi}\,\frac{1}{J_{K+2}^2(\varkappa\rho_{\rm ch}) + N_{K+2}^2(\varkappa\rho_{\rm ch})}. \qquad (9)$$

Then the value $\rho_{\rm ch} \approx 40$ fm is obtained. So, the radial range, which can be interpreted as an "internal region" in the case of the virtual three-body state, is huge.

The dependence of the width (defined as FWHM) on resonance energy is shown in Fig. 7 for $[s_{1/2}]^2$ and $[p_{1/2}]^2$ resonance peaks. The variation of energy in each case is obtained by the respective variation of parameters of the s- and p-wave interactions. The $[p_{1/2}]^2$ curve is obtained in calculations with a broad source. The curves for $[s_{1/2}]^2$ calculations practically coincide for broad and narrow source calculations; this independence is an expected result for such a narrow structure. It can be seen in Fig. 7 that the curve for

[2]What is called the "Borromean" property of resonances, due to the relation to artificially created Borromean states in the ACCC method [20], is better characterized as the energy condition of a "true three-body decay" or a "democratic decay." The detailed discussion of three-body decay modes can be found in Ref. [23].

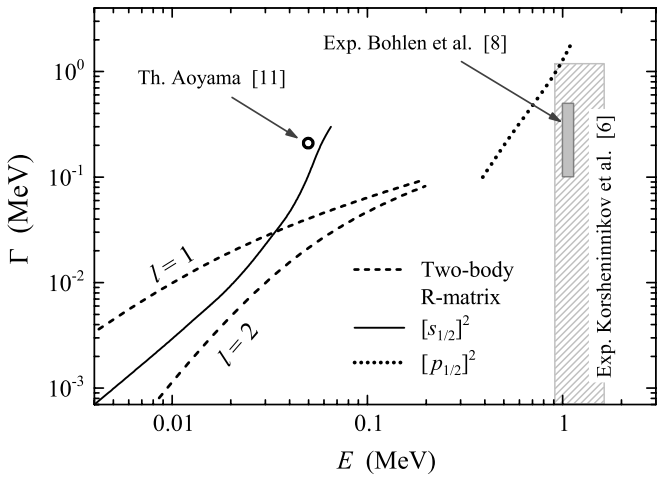

FIG. 7. Width as a function of resonance energy for $[s_{1/2}]^2$ and $[p_{1/2}]^2$ states. Standard two-body R-matrix estimates are shown for $l = 1$ and $l = 2$ (channel radius 40 fm) by dashed curves. Possible experimental ranges according to experiments in Refs. [6,8] are shown by hatched and gray rectangles correspondingly. The result of theoretical prediction [11] is shown by a small circle. The curve for the $[p_{1/2}]^2$ state is calculated with the broad source. Calculations for the $[s_{1/2}]^2$ state with broad and narrow sources practically coincide within the shown energy range.

the $[s_{1/2}]^2$ state stays mainly in between standard two-body R-matrix estimates with $l = 1, l = 2$ (channel radius 40 fm) as an "effective angular momentum" for $K = 0$ is $\mathcal{L} = 3/2$. The obtained dependence is in a good agreement with the ^{10}He ground state prediction by Aoyama [11] which gave $E = 0.05$ MeV and $\Gamma = 0.21$ MeV (small circle in Fig. 7). We think that this agreement is an important fact demonstrating the stability of the theoretical results on this issue, because very different theoretical models and different p-wave interactions were employed in the studies of Ref. [11].

The point about the peripheral character of the $[s_{1/2}]^2$ state is also confirmed by analysis of the correlation density. The correlation densities $|\Psi^{(+)}|^2$ for the ^{10}He WFs on the $\{\rho, \theta_\rho\}$ plane are shown in Fig. 8. The θ_ρ hyperspherical variable describes the distribution between X and Y subsystems. It is a component of the five-dimensional hyperangle $\Omega_\rho = \{\theta_\rho, \Omega_x, \Omega_y\}$. For ^{10}He in the "T" Jacobi system,

$$X = \sqrt{2}\rho \sin\theta_\rho, \quad Y = \sqrt{5/8}\rho \cos\theta_\rho.$$

Some properties of the three-body virtual state are well illustrated by this plot.

(i) The $[s_{1/2}]^2$ and $[p_{1/2}]^2$ configurations demonstrate very different correlations in the internal region and on the asymptotic. While in the $[s_{1/2}]^2$ case the distributions are expectedly quite featureless, in the $[p_{1/2}]^2$ case we observe in the internal region the double-humped structures—"dineutron" and "cigar"—in the variable θ_ρ, which are connected to so-called Pauli focusing [Figs. 8(b), 8(c); in case 8(b), only the "dineutron" peak is seen]. These structures are well known from the studies of the other p-shell nuclei [25]. When there is no attractive s-wave interaction in the ^{8}He-n channel [Fig. 8(c)], this double-humped correlation "survives" up to the asymptotic region in a somewhat modified form and thus could possibly be observed in experiment (see also the discussion in Sec. IV B).

(ii) As for the peripheral character of the $[s_{1/2}]^2$ WF, a comparison of Figs. 8(b) and 8(c) indicates that the double-humped structure connected to $[p_{1/2}]^2$ configurations is sharply concentrated in the internal region ($\rho \sim 7$ fm) and rapidly decreases beyond 10–15 fm. In contrast, the $[s_{1/2}]^2$ WF is peaked at $\rho \sim 15$ fm and extends smoothly to around 50 fm [Fig. 8(a)]. Distance $\rho \sim 15$ is well beyond the typical nuclear size; for configurations with such typical ρ values, the individual valence nucleons have on average a 10 fm distance to the core.

(iii) Radial stabilization of the $[s_{1/2}]^2$ WF (the distances at which the $\sim \exp[i\varkappa\rho]$ behavior is mainly achieved) is

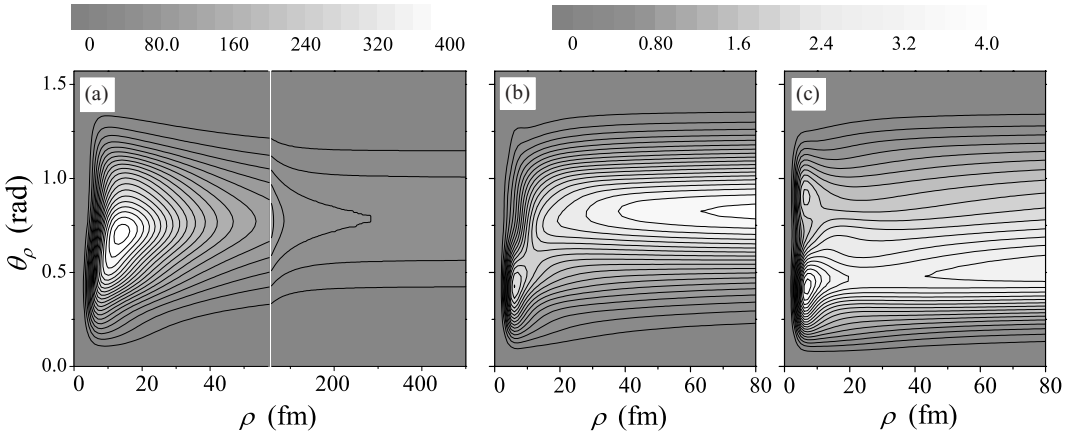

FIG. 8. Correlation density $|\Psi^{(+)}|^2$ for the ^{10}He WF on the $\{\rho, \theta_\rho\}$ plane in the "T" Jacobi system. (a) Case of strong three-body virtual state $V_c^0 = -26.93$ ($a = -15$ fm), $V_c^1 = -4.5$ MeV for energy taken on peak position ($E = 4$ keV); see also Fig. 2(b). (b) Same as (a) but for $E = 2.3$ MeV (the latter energy is the expected position for peak in the case of a state with $[p_{1/2}]^2$ structure). (c) State with $[p_{1/2}]^2$ structure $V_c^0 = 0$, $V_c^1 = -4.5$ MeV. Calculations are made with the narrow source; energy is taken on the peak position ($E = 2.3$ MeV).

taking place at quite large distances [$\rho \approx 300$–400 fm, see Fig. 8(a)]. This is connected to both a very low energy of the peak (4 keV in this particular calculation) and an effectively long-range character of interactions in the s-wave ^{8}He-n channel, responsible for the formation of the three-body virtual state.

(iv) One can see from Fig. 5(c) that the cross section behavior in the energy region of the $[p_{1/2}]^2$ state ($E \approx 2$–3 MeV) is practically not sensitive to the low-energy behavior of the spectrum (presence or absence of the $[s_{1/2}]^2$ state). It is thus possible to think that these configurations are practically independent in this energy region. A comparison of Figs. 8(b) and 8(c) shows that this is not true. Both the internal structure of the WF and correlations for decay products demonstrate strong sensitivity to the presence of the $[s_{1/2}]^2$ state, although it is not clearly seen in the total production cross section in this energy range.

An important technical insight could be obtained from the behavior of the effective hyperspherical interactions [Eq. (5)]. In Fig. 9, we show the "most attractive" diagonal potential (this appears to to be the $K = 0$ term in all the cases) and the lowest diagonalized potential. The latter can be considered as an effective interaction for some simple adiabatic approximation to the problem, which is qualitatively illustrative but quantitatively could be not very reliable. The important dynamical aspects which become clear from these plots have already been discussed in our work [14] on the example of broad states of the ^{5}H system. It can be seen in Fig. 9 that even the "most attractive" diagonal potentials are in reality repulsive and do not even show any sign of "pocket" formation. The structures in the continuum are formed here only by interaction of multiple channels. It is interesting to note that the possibility of this class of states was discussed many years ago (as so-called "resonances of the second kind" [26]) but now we seem to face them systematically in the few-body drip-line nuclei.

In the broad range of the resonance energies, the state is located above the effective barrier top. Formation of the peaks, which could be very narrow (see Figs. 5 and 7) is presumably connected here not with barrier penetration but with slow motion above the barrier and reflection from the right slope of the barrier.[3] Only in the extreme low-energy case [Fig. 9(c)], the process could be interpreted as penetration through the effective barrier. Typical range of the barrier is consistent in this case with the "channel radius" estimates by Eq. (9).

TABLE I. Internal structure of the virtual three-body state and the bound ^{10}He states close to the ^{8}He+n+n threshold.

E (MeV)	$[s_{1/2}]^2$	$[p_{1/2}]^2$	$[p_{3/2}]^2$	$[d]^2$
0.04[a]	93.3	2.2	1.8	1.8
−0.06[b]	66.1	23.8	4.7	4.2
−0.3[c]	51.0	35.9	6.1	5.7

[a]Calculation of Fig. 5(c), short-dashed curve ($V_c^0 = -25.82$ MeV, $a = -10$ fm, $V_c^1 = -4.5$ MeV). Radius for internal normalization was taken as $\rho_{\text{int}} = 40$ fm, see Fig. 8(a).
[b]Continuum above this bound state is shown in Figs. 5(a) and 5(d) by the short-dashed curves ($V_c^0 = -25.82$ MeV, $a = -10$ fm, $V_c^1 = -10$ MeV).
[c]The same calculation as described for $E = -0.06$ MeV, but with extra binding added by the attractive three-body potential.

The evolution of the nuclear structure near the threshold is also an interesting question, which is briefly discussed below. The short-dash curves ($V_c^0 = -25.82$ MeV, $a = -10$ fm) in Figs. 5(a) and 5(d) show qualitatively different behavior compared to the expected sharpening of the threshold peak. It happens because in this case the bound 0^+ state of ^{10}He is formed with a binding energy ≈60 keV. Therefore these curves do not represent a valid result in the context of our studies (we should consider only the three-body Hamiltonians which do not lead to the bound ^{10}He). However, it is interesting to see how the nuclear structure evolves in this case (Table I). The virtual three-body state shows strong domination of the $[s_{1/2}]^2$ component in the internal region (the first row in Table I). As soon as the state becomes bound, the structure changes drastically with rapid increase of the $[p_{1/2}]^2$ configuration weight (see the second row in Table I).

[3]The attractive potentials with barriers are not necessarily needed to form resonances in the continuum. They can be formed by pure repulsive potentials with broad "shelves."

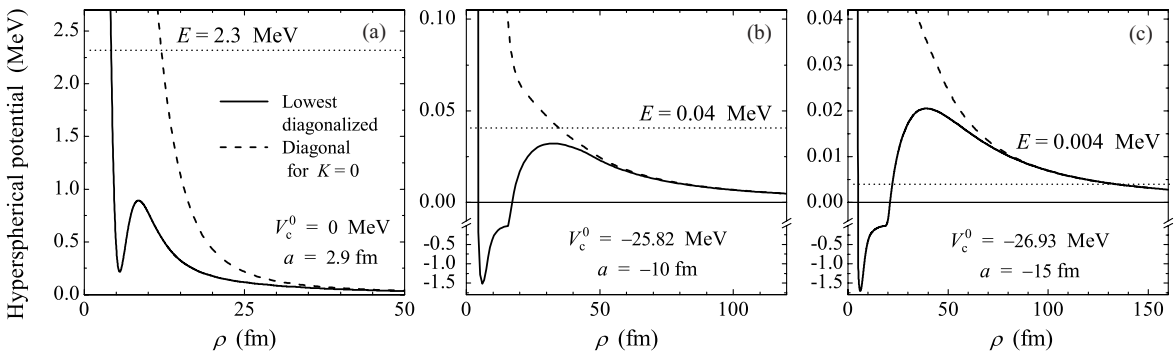

FIG. 9. Hyperspherical potentials [Eq. (5)] as functions of hyperradius. Solid line shows the lowest diagonalized potential; dashed line, the lowest diagonal potential (in all the cases, this is the $K = 0$ term). (a) The $[p_{1/2}]^2$ state at $E = 2.3$ MeV [see solid curves in Figs. 5(c) and 5(f)]. Panels (b) and (c) correspond to $[s_{1/2}]^2$ states at $E = 0.04$ MeV [see short-dashed curves in Figs. 5(c) and 5(f)] and at $E = 0.004$ MeV, respectively.

If we bind the ^{10}He even more strongly, so that the binding energy becomes 0.3 MeV, which corresponds to the binding energy of ^{11}Li, its structure begins to resemble closely the typical structure of ^{11}Li with practically equal population of the $[s_{1/2}]^2$ and $[p_{1/2}]^2$ configurations (the third row in Table I). So, the bound analog of the virtual three-body state is expected to be not a state with dominant $[s_{1/2}]^2$ configuration, but rather a state with strong "competition" between the s-wave and p-wave configurations. Usually the structure of narrow resonant (or quasibound) states is characterized by a high identity with the structure of the corresponding bound states.[4] The virtual three-body state demonstrates the behavior, which is qualitatively different in this respect.

From the presented results, we can probably conclude that in terms of nuclear dynamics, a three-body virtual state is intermediate between a two-body virtual state and an ordinary resonance.

F. Consistence with 3 → 3 scattering calculations

The model cross section calculations for realistic ^{9}He energies [Figs. 5(c) and 5(f)] show very diverse results in the case of narrow and broad sources. The question can be asked, then, what should be considered as a "real" position of the ^{10}He g.s. and whether it is at all reasonable to speak about such real positions if diverse experimental responses could be expected. The theoretical approach which is "neutral" with respect to a possible reaction mechanism is represented by 3 → 3 scattering calculations.

Figures 10 and 11 show the results of the 3 → 3 scattering calculations for a pure $[p_{1/2}]^2$ state and in the presence of a low-energy $[s_{1/2}]^2$ state, respectively. The details of the approach can be found in Ref. [27] for the example of the ^{5}H nucleus. The three-body Hamiltonian here is the same as in Figs. 5(c) and 5(f). Three different values are displayed for these calculations: the diagonal 3 → 3 scattering phase shifts, the first diagonalized phase shift (so called eigenphase), and the diagonal internal normalizations for scattering WFs, i.e.,

$$N_{\rho_{\rm int}}(E) = \frac{1}{\varkappa^5} \sum_{K\gamma} \int_0^{\rho_{\rm int}} d\rho \left| \chi^{K\gamma}_{K\gamma}(\varkappa\rho) \right|^2. \qquad (10)$$

The size of the "internal region" $\rho_{\rm int} = 6$ fm was taken for this value as in Ref. [27].

For $[p_{1/2}]^2$ state the 3 → 3 calculations in Fig. 10 give somewhat different resonant energies for different responses: $E = 1.8$ MeV for internal normalization, $E \sim 2$ MeV for the most strongly changing diagonal phase shifts, and $E = 2.3$ for the eigenphase. Such spread is clearly related to the fact that the phase shifts barely pass 90°. So, we can speak about a resonant energy of about $E \sim 2.0$–2.3 MeV, when only scattering is concerned. The agreement of 3 → 3 calculations with the narrow source calculations is reasonable. That could be an indication that "ordinary" reactions (simulated in this model) are a more preferable tool for accessing properties of ^{10}He than are reactions with exotic nuclei (such as ^{11}Li).

For narrow low-lying $[s_{1/2}]^2$ state (shown in Fig. 11), the results provided by all 3 → 3 calculations (resonance energy

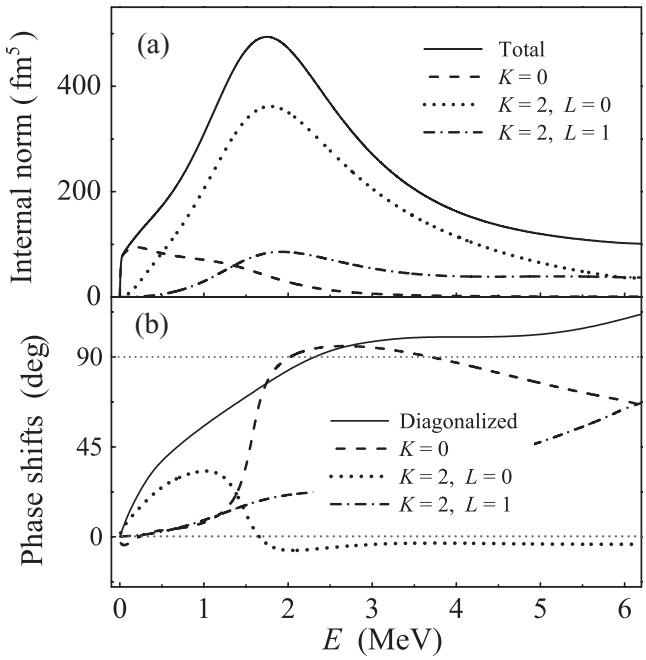

FIG. 10. 3 → 3 scattering calculations, $V_c^0 = 0$, $V_c^1 = -4.5$ MeV. (a) Internal normalizations [Eq. (10)] for dominant components of the WF. (b) Diagonalized phase shift (eigenphase), solid curve; diagonal phase shifts for the lowest hyperspherical components, other curves (see legend).

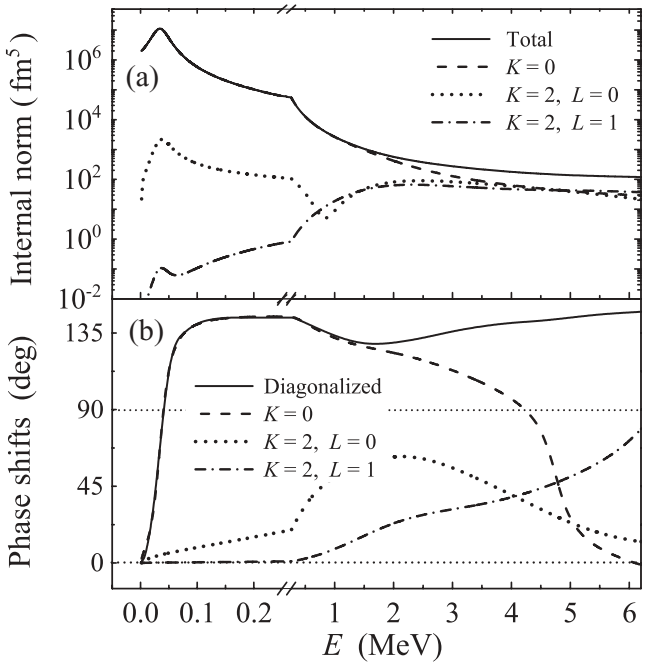

FIG. 11. Same as Fig. 10, but for $V_c^0 = -25.82$ MeV ($a = -10$ fm), $V_c^1 = -4.5$ MeV.

[4] A good example is the structure of the bound and quasibound states—isobaric partners. An exception here is the situation of the Thomas-Ehrmann shift, when significant deviations from isobaric symmetry can be observed.

$E = 40$ keV) are in excellent agreement with each other and with previous model calculations [Figs. 5(c) and 5(f), curves with $a = -10$ fm]. This state is formed exclusively by the $K = 0$ WF component. An evidence for the $[p_{1/2}]^2$ state contributions could be found in the phase shift at around 2 MeV, but it is not very well expressed. Better evidence is provided by internal normalizations for $K = 2$ components of the WF. These show a maximum at about 2.3 MeV and provide much broader structures than in the case of the $[p_{1/2}]^2$ state not affected by the $[s_{1/2}]^2$ configuration (Fig. 10). Again, we can come to the conclusion that the $[p_{1/2}]^2$ state survives in the presence of the $[s_{1/2}]^2$ state in a somewhat modified (shifted up and broadened) form, but the population of it is expected to be poor.

IV. DISCUSSION

A. What is the ground state of ^{10}He?

It was proposed in Ref. [11] that the state of ^{10}He observed so far is not the ground but the first excited state with a $[p_{1/2}]^2$ structure, while the ground $[s_{1/2}]^2$ state remains unobserved. We confirm here the finding of Ref. [11] that for considerable s-wave attraction in the ^{9}He subsystem, two 0^+ states with different structures should coexist in the low-energy spectrum of ^{10}He. However, we also find that population of the $[s_{1/2}]^2$ configuration (in the case of a strong s-wave attraction in ^{9}He and realistic reaction scenario) is always very pronounced compared to the $[p_{1/2}]^2$ configuration. For that reason, we can expect that if the $[s_{1/2}]^2$ state *really exists* then the $[p_{1/2}]^2$ component is difficult to observe in experiment (as it is lost on a "nonresonant background" of $[s_{1/2}]^2$ low-energy excitation). It can be found that the energy position of the $[p_{1/2}]^2$ component of 0^+ state is quite stable when the s-wave attraction is increased. However, for extreme cases of the s-wave attraction, this contribution becomes much broader and in general "lost" on a thick right "tail" of the $[s_{1/2}]^2$ ground state.

Current experimental situation in ^{10}He is clearly not in favor of the existence of the $[s_{1/2}]^2$ state. Several theoretical spectra of ^{10}He are provided in Fig. 12 on top of the experimental data from Ref. [6]. Theoretical curves are convoluted with the energy resolution of the experiment [6] which is parametrized as $\Delta E = 0.7\sqrt{E}$ (ΔE is FWHM). The calculation with the ^{9}He subsystem having $p_{1/2}$ g.s. at about 2 MeV reasonably fits the data. The experimental cross section peaked at about 1.2 MeV could be consistent with some range of p-wave interactions for the ^{11}Li source [Figs. 5(e) and 5(f)]. This, however, is possible only for quite a weak attractive part of the s-wave potential: $V_c^0 > -20$ MeV. For such parameter values, the s-wave interaction is in general still effectively repulsive (due to a large repulsive core). For that reason, if we completely rely on the data [6], we would impose a theoretical limit of $a > -5$ fm for the ^{8}He-n scattering length. The derived theoretical limit is in strong contradiction with the *upper* limit for the scattering length in ^{9}He, i.e., $a < -10$ fm, imposed in the experiment [10]. There is no contradiction between our theoretical limit and the data [12] which provided a *lower* limit of $a > -20$ fm for scattering length.

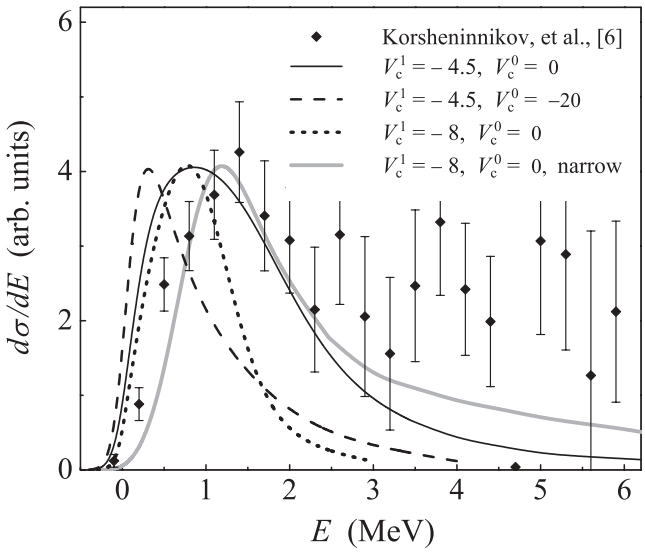

FIG. 12. Calculation results convoluted with experimental resolution of Ref. [6] and experimental data. Solid, dashed, and dotted curves correspond to calculations with ^{11}Li source [see Figs. 5(f) solid, 5(f) dotted, and 5(e) solid curves]. Gray line shows calculation with narrow source [Fig. 5(b) dotted curve].

The unclear situation with the exotic reaction mechanism expected for reactions with ^{11}Li could have been resolved by a different experimental approach. Such an experiment in principle exists: the ground state of ^{10}He and two excited states were identified in the complicated $2p$-$2n$ exchange reaction ^{10}Be(^{14}C,^{14}O)^{10}He [7,8]. Unfortunately, the observed peaks rest on a "thick" background and have a low statistical confidence. None of our calculations are consistent with the results of this experiment. Namely, we cannot reproduce in any model assumption the small width of the g.s. obtained in that work (300 ± 200 keV at 1.07 MeV of excitation). For example, in Fig. 5(b), the width of the state found at about 1.1 MeV is $\Gamma \sim 1.1$ MeV (see also Fig. 7). A smaller width of the ^{10}He g.s. *if it takes place in reality* should mean a non-single-particle nature of this state [i.e., it is not described as ^{8}He(g.s.)+n+n] and hence a limited applicability of our model.

B. Prospects of correlation studies

Important structure information about the three-body system could be obtained analyzing the correlations among the decay products. Recent examples of such data analysis include successful application to the broad states in the continuum of the ^{5}H system [28] and to the two-proton radioactivity decays of ^{19}Mg [29] and ^{45}Fe [30]. Such range of application indicates the potential power of the correlation studies.

The partial decompositions of the cross section given in Fig. 6 show how the contributions of the $[s_{1/2}]^2$ component (mainly $K = 0$) and $[p_{1/2}]^2$ component (mainly $K = 2$) change when we add the s-wave interaction in ^{9}He channel on top of the p-wave interaction or switch from the narrow to the broad source. The qualitative differences in these decompositions should be seen as qualitative differences in the correlation patterns.

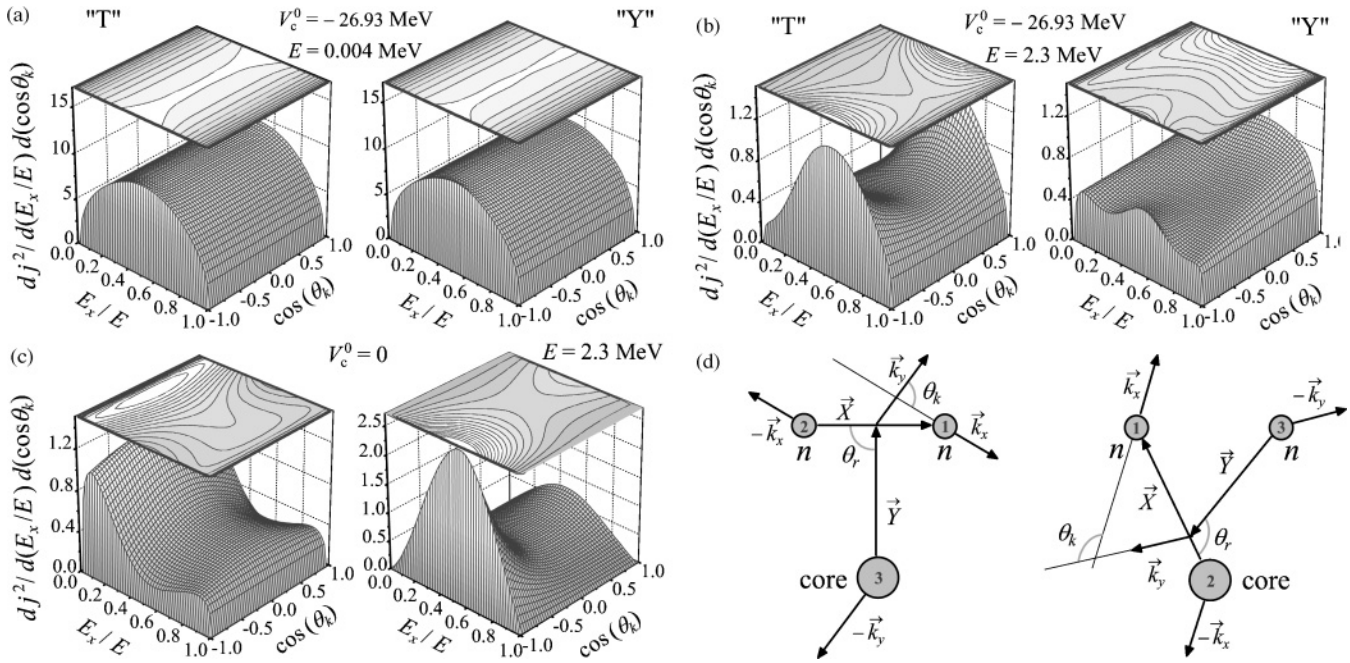

FIG. 13. Complete correlation information about decays of 0^+ state at given energy E. Left and right columns show the same result in "T" and "Y" Jacobi systems. Calculations provided in panels (a), (b), and (c) correspond to the same panels of Fig. 8. Panel (d) shows the coordinates and angles in radial and momentum space for the "T" and "Y" Jacobi systems.

The complete correlation information is provided in Fig. 13 for correlations in the $[s_{1/2}]^2$ state [$E = 4$ keV, Fig. 13(a)] and in the $[p_{1/2}]^2$ state at $E = 2.3$ MeV in the calculations with attraction in s-wave [Fig. 13(b)] and no s-wave attraction [Fig. 13(c)]. The correlation densities are given in the plane of parameters $\{\varepsilon, \cos(\theta_k)\}$ both in "T" and "Y" Jacobi coordinate systems. Parameter $\varepsilon = E_x/E$ describes the energy distribution between the X and Y Jacobi subsystems (E_x is energy in the X Jacobi subsystem). Parameter θ_k is the angle between Jacobi momenta k_x and k_y in the chosen Jacobi coordinate system:

$$\cos(\theta_k) = \frac{(\mathbf{k}_x, \mathbf{k}_y)}{k_x\, k_y}.$$

More details can be found in Ref. [31].

The correlation picture for the virtual three-body state with the $[s_{1/2}]^2$ structure is quite featureless [Fig. 13(a)]. The energy distribution between subsystems is close to the "phase volume" distribution

$$\frac{d^2\sigma}{dE dE_x} \sim E\,\sqrt{E_x(E - E_x)}. \qquad (11)$$

There are only minor deviations from a flat distribution for $\cos(\theta_k)$ at $\theta_k \sim 0^\circ$ and $\theta_k \sim 180^\circ$ in the "T" Jacobi system (these are configurations in which three particles come out in a line).

The predicted correlations for the $[p_{1/2}]^2$ state in the "T" Jacobi system [Fig. 13(c)] look very much like those already observed in other p-wave systems of ^{6}Be [32] and ^{5}H [28]. There is a double-hump structure reflecting the $[p_{1/2}]^2$ population. The hump, which corresponds to low-energy motion between neutrons, is strongly enhanced because of the final state interaction (FSI) in the n-n channel.

Figure 13(b) provides a prediction of correlations which may be important for prospective ^{10}He studies. If the attractive s-wave interaction is added, it qualitatively changes the picture of correlations at the expected $[p_{1/2}]^2$ state position. Now the energy distribution between subsystems (in the "T" Jacobi system) is close to the phase-space distribution in Eq. (11). Also, the angular distribution changes drastically: the correlation density is concentrated in the regions where one of the neutrons is close to the ^{8}He core in the momentum space [$\cos(\theta_k) \sim \pm 1$ and $E_x/E \sim 5/9$ in the "T" Jacobi system]. In this case, the only expressed feature in the "Y" Jacobi system is the "dineutron" correlation, which can be seen as a small peak at $\cos(\theta_k) \sim -1$ and $E_x/E \sim 1/2$.

The drastic changes between distributions in Figs. 13(b) and 13(c) mean that in experimental measurements giving access to such a characteristic, there will be no doubt in the structure identification even in the case of a poor population of the low-energy part of the spectrum or technical problems with detection of the low-energy events.

C. Reliability of the results

It should be mentioned once again that the aspects of the ^{10}He dynamics discussed in this work are only valid if the single-particle ^{8}He(g.s.)+n+n structure of the low-lying ^{10}He states really takes place. The basis for such an assumption is provided by knowledge of the ^{9}He spectrum. However, the narrow first resonant states of ^{9}He, as observed in Refs. [3,4] [$E(p_{1/2}) = 1.27$ MeV, $\Gamma = 0.1$ MeV, and

TABLE II. Paring energy (in MeV) for ^{10}He defined as $E_p = S_{2n} - 2S_n$ calculated in different theoretical approaches.

Work	[2]	[5][a]	[34]	[35]	[11]	[36][b]	This work[a]
$-S_n$	1.22	0.74	0.84	2.38	1.27	1.60	2.0
$-S_{2n}$	1.18	0.6	1.09	2.78	1.68	1.94	∼2.0–2.3
E_p	1.26	0.88	0.59	1.98	0.86	1.25	∼1.7–2.0

[a]We use $p_{1/2}$ elastic cross section peak energy to define S_n.
[b]See Table 1, column 6 of Ref. [36].

$E(p_{3/2}) = 2.4$ MeV, $\Gamma = 0.7$ MeV], presume that it is not true, because small spectroscopic factors are expected [33]. In the case that the results of Ref. [12] are preferable [$E(p_{1/2}) = 2$ MeV, $\Gamma = 2$ MeV], implying that this is a single-particle state, the basis for our model becomes reliable.

Sensitivity of the predictions to the s-wave interaction in the ^{9}He channel is very high. The experimental results of Refs. [10] ($a < -10$ fm) and [12] ($a > -20$ fm) are not contradictory, although not too restrictive. Thus, still no solid experimental ground can be found here. We think that this issue is a key point for understanding the ^{10}He structure.

An important conclusion of these studies is that the energy spectrum obtained in experiments with ^{11}Li is strongly affected by the reaction mechanism, and we do not reproduce the results of the experiment [6] without taking this effect into account. The question can be raised from the theoretical side of how reliable is the statement that for the $p_{1/2}$ state in ^{9}He at about 2 MeV, we cannot get a *state* in ^{10}He at 1.2 MeV straightforwardly. In Table II, we list paring energies E_p for valence neutrons calculated for ^{10}He in different theoretical approaches. With the $p_{1/2}$ state at 2 MeV, the paring energy should be about 2.8 MeV, while in various theoretical approaches, it is typically around 1 and never exceeds 2 MeV. It is clear that relatively small paring energy in ^{10}He is common for different theoretical models and can be considered as a reliable prediction. Also, if we look at the nearby isotopes, for the $p_{3/2}$ subshell nuclei ^{6}He and ^{8}He, E_p is 2.6 and 3.04 MeV, respectively. For ^{11}Li, where the $p_{1/2}$ subshell is populated, the paring energy is known to be small: $E_p \sim 0.8$ MeV.

V. CONCLUSION

We would like to emphasize the most important results of our studies:

(i) Within the theoretical model for the $p_{1/2}$ state in ^{9}He located at about 2 MeV, it is problematic to straightforwardly obtain the ^{10}He g.s. at about 1.2 MeV. The value of paring energy, which is required for that, is 2.8 MeV; while for the $[p_{1/2}]^2$ configuration, it is typically ∼1–2 MeV.

(ii) The attraction in the s wave allows the shift of the state with the $[p_{1/2}]^2$ configuration to a significantly lower energy. However, some extreme values of attraction ($a \leqslant -5$ fm) lead to the formation of a low-energy $[s_{1/2}]^2$ state, which is seen as a sharp peak in the cross section at energies less than 0.3 MeV. The appearance of such a state is in accord with predictions of Ref. [11].

(iii) In contrast to the approach of Ref. [11], we study the conditions of "coexistence" of $[s_{1/2}]^2$ and $[p_{1/2}]^2$ states in the 0^+ continuum for realistic scenarios. It is shown that the state with the $[p_{1/2}]^2$ structure is poorly populated (also suffer significant broadening) in the presence of the $[s_{1/2}]^2$ ground state and can be easily lost (small on the s-wave "background"). For that reason, our studies do not support the idea of Ref. [11] that the ground $[s_{1/2}]^2$ state of the ^{10}He remains unobserved, while the state observed so far is the first excited one with $[p_{1/2}]^2$ structure.

Concerning comparison with experimental data:

(i) Observation of quite a broad peak in ^{10}He at about 1.2 MeV in Ref. [6] could be explained by a specific mechanism of the chosen reaction induced by ^{11}Li (namely, the huge size of the neutron halo in ^{11}Li). This explanation is possible only in the case of absence of the virtual state in the ^{9}He channel. For the ^{10}He ground $[p_{1/2}]^2$ state located at $E \geqslant 2$ MeV, the mentioned reaction mechanism leads to a strong enhancement of the low-energy transition strength even without any significant attraction in the s wave. As a result, the peak in the cross section may be shifted to a lower energy (e.g., ∼1.2 MeV).

(ii) The provided theoretical model essentially infers the properties of the ^{10}He system based on the properties of the ^{9}He subsystem. At the moment we cannot make the existing data on ^{9}He and ^{10}He consistent within this model. Calculations with a large negative scattering length (e.g., $a < -5$ fm; experimental limit [10] is $a < -10$ fm) in the core-n subsystem necessarily lead to the formation of the single narrow peak below 0.3 MeV in the spectrum which should have been seen in the experiment [6].

(iii) We have to conclude that the existing experimental data do not allow one to establish unambiguously the "real" g.s. position for ^{10}He. Alternative experiments (relative to those utilizing ^{11}Li beams) are desirable. Further clarification of the controversy between the ^{9}He and ^{10}He spectra is indispensable for gaining a theoretical understanding of the helium isobar properties.

ACKNOWLEDGMENTS

We are grateful to Prof. Yu. Ts. Oganessian for inspiration for this work. We are grateful to Profs. A. A. Korsheninnikov, G. M. Ter-Akopian, and M. S. Golovkov for their careful reading of the manuscript and valuable discussions. L.V.G. is supported by the German DFG Grant 436 RUS 113/907/0-1, INTAS Grant 05-1000008-8272, Russian RFBR Grants 05-02-16404 and 05-02-17535, and Russian Ministry of Industry and Science Grant NS-1885.2003.2.

[1] A. I. Baz, V. F. Demin, and M. V. Zhukov, Sov. J. Nucl. Phys. **9**, 693 (1969) [Yad. Fiz. **9**, 1184 (1969)].

[2] J. Stevenson, B. A. Brown, Y. Chen, J. Clayton, E. Kashy, D. Mikolas, J. Nolen, M. Samuel, B. Sherrill, J. S. Winfield, Z. Q. Xie, R. E. Julies, and W. A. Richter, Phys. Rev. C **37**, 2220 (1988).

[3] K. K. Seth, M. Artuso, D. Barlow, S. Iversen, M. Kaletka, H. Nann, B. Parker, and R. Soundranayagam, Phys. Rev. Lett. **58**, 1930 (1987).

[4] H. G. Bohlen, B. Gebauer, D. Kolbert, W. von Oertzen, E. Stiliaris, M. Wilpert, and T. Wilpert, Z. Phys. A **330**, 227 (1988).

[5] A. A. Korsheninnikov, B. V. Danilin, and M. V. Zhukov, Nucl. Phys. **A559**, 208 (1993).

[6] A. A. Korsheninnikov, K. Yoshida, D. V. Aleksandrov, N. Aoi, Y. Doki, N. Inabe, M. Fujimaki, T. Kobayashi, H. Kumagai, C.-B. Moon, E. Yu. Nikolskii, M. M. Obuti, A. A. Ogloblin, A. Ozawa, S. Shimoura, T. Suzuki, I. Tanihata, Y. Watanabe, and M. Yanokura, Phys. Lett. **B326**, 31 (1994).

[7] A. N. Ostrowski, H. G. Bohlen, B. Gebauer, S. M. Grimes, R. Kalpakchieva, Th. Kirchner, T. N. Massey, W. von Oertzen, Th. Stolla, M. Wilpert, and Th. Wilpert, Phys. Lett. **B338**, 13 (1994).

[8] H. G. Bohlen, A. Blazevic, B. Gebauer, W. Von Oertzen, S. Thummerer, R. Kalpakchieva, S. M. Grimes, and T. N. Massey, Prog. Part. Nucl. Phys. **42**, 17 (1999).

[9] T. Kobayashi, K. Yoshida, A. Ozawa, I. Tanihata, A. Korsheninnikov, E. Nikolski, and T. Nakamura, Nucl. Phys. **A616**, 223c (1997).

[10] L. Chen, B. Blank, B. A. Brown, M. Chartier, A. Galonsky, P. G. Hansen, and M. Thoennessen, Phys. Lett. **B505**, 21 (2001).

[11] S. Aoyama, Phys. Rev. Lett. **89**, 052501 (2002).

[12] M. S. Golovkov, L. V. Grigorenko, A. S. Fomichev, A. V. Gorshkov, V. A. Gorshkov, S. A. Krupko, Yu. Ts. Oganessian, A. M. Rodin, S. I. Sidorchuk, R. S. Slepnev, S. V. Stepantsov, G. M. Ter-Akopian, R. Wolski, A. A. Korsheninnikov, E. Yu. Nikolskii, V. A. Kuzmin, B. G. Novatskii, D. N. Stepanov, P. Roussel-Chomaz, and W. Mittig, Phys. Rev. C **76**, 021605(R) (2007).

[13] D. Gogny, P. Pires, and R. de Tourreil, Phys. Lett. **B32**, 591 (1970).

[14] L. V. Grigorenko, N. K. Timofeyuk, and M. V. Zhukov, Eur. Phys. J. A **19**, 187 (2004).

[15] R. J. Ascuitto and N. K. Glendenning, Phys. Rev. **181**, 1396 (1969).

[16] N. B. Shulgina (private communication).

[17] L. V. Grigorenko and M. V. Zhukov, Phys. Rev. C **76**, 014008 (2007).

[18] B. V. Danilin, J. S. Vaagen, T. Rogde, S. N. Ershov, I. J. Thompson, and M. V. Zhukov, Phys. Rev. C **76**, 064612 (2007).

[19] W. Glöckle, Phys. Rev. C **18**, 564 (1978).

[20] N. Tanaka, Y. Suzuki, K. Varga, and R. G. Lovas, Phys. Rev. C **59**, 1391 (1999).

[21] A. Delfino, T. Frederico, and L. Tomio, Few-Body Syst. **28**, 259 (2000).

[22] T. Frederico and M. T. Yamashita, Nucl. Phys. **A790**, 116c (2007).

[23] L. V. Grigorenko, R. C. Johnson, I. G. Mukha, I. J. Thompson, and M. V. Zhukov, Phys. Rev. C **64**, 054002 (2001).

[24] M. S. Golovkov, L. V. Grigorenko, A. S. Fomichev, Yu. Ts. Oganessian, Yu. I. Orlov, A. M. Rodin, S. I. Sidorchuk, R. S. Slepnev, S. V. Stepantsov, G. M. Ter-Akopian, and R. Wolski, Phys. Lett. **B588**, 163 (2004).

[25] M. V. Zhukov, B. V. Danilin, D. V. Fedorov, J. M. Bang, I. J. Thompson, and J. S. Vaagen, Phys. Rep. **231**, 151 (1993).

[26] A. I. Baz, Zh. Eksp. Teor. Fiz. **70**, 397 (1976).

[27] N. B. Shulgina, B. V. Danilin, L. V. Grigorenko, M. V. Zhukov, and J. M. Bang, Phys. Rev. C **62**, 014312 (2000).

[28] M. S. Golovkov, L. V. Grigorenko, A. S. Fomichev, S. A. Krupko, Yu. Ts. Oganessian, A. M. Rodin, S. I. Sidorchuk, R. S. Slepnev, S. V. Stepantsov, G. M. Ter-Akopian, R. Wolski, M. G. Itkis, A. S. Denikin, A. A. Bogatchev, N. A. Kondratiev, E. M. Kozulin, A. A. Korsheninnikov, E. Yu. Nikolskii, P. Roussel-Chomaz, W. Mittig, R. Palit, V. Bouchat, V. Kinnard, T. Materna, F. Hanappe, O. Dorvaux, L. Stuttgé, C. Angulo, V. Lapoux, R. Raabe, L. Nalpas, A. A. Yukhimchuk, V. V. Perevozchikov, Yu. I. Vinogradov, S. K. Grishechkin, and S. V. Zlatoustovskiy, Phys. Rev. C **72**, 064612 (2005).

[29] I. Mukha, K. Sümmerer, L. Acosta, M. A. G. Alvarez, E. Casarejos, A. Chatillon, D. Cortina Gil, J. Espino, A. Fomichev, J. E. Garca-Ramos, H. Geissel, J. Gomez-Camacho, L. Grigorenko, J. Hoffman, O. Kiselev, A. Korsheninnikov, N. Kurz, Yu. Litvinov, I. Martel, C. Nociforo, W. Ott, M. Pfutzner, C. Rodrguez-Tajes, E. Roeckl, M. Stanoiu, H. Weick, and P. J. Woods, Phys. Rev. Lett. **99**, 182501 (2007).

[30] K. Miernik, W. Dominik, Z. Janas, M. Pfützner, L. Grigorenko, C. R. Bingham, H. Czyrkowski, M. Cwiok, I. G. Darby, R. Dabrowski, T. Ginter, R. Grzywacz, M. Karny, A. Korgul, W. Kusmierz, S. N. Liddick, M. Rajabali, K. Rykaczewski, and A. Stolz, Phys. Rev. Lett. **99**, 192501 (2007).

[31] L. V. Grigorenko and M. V. Zhukov, Phys. Rev. C **68**, 054005 (2003).

[32] O. V. Bochkarev, A. A. Korsheninnikov, E. A. Kuz'min, I. G. Mukha, L. V. Chulkov, and G. B. Yan'kov, Nucl. Phys. **A505**, 215 (1989).

[33] F. C. Barker, Nucl. Phys. **A741**, 42 (2004).

[34] Y. S. Shen and Z. Ren, Phys. Rev. C **54**, 1158 (1996).

[35] P. Navratil and B. R. Barrett, Phys. Rev. C **57**, 3119 (1998).

[36] A. Volya and V. Zelevinsky, Phys. Rev. Lett. **94**, 052501 (2005).